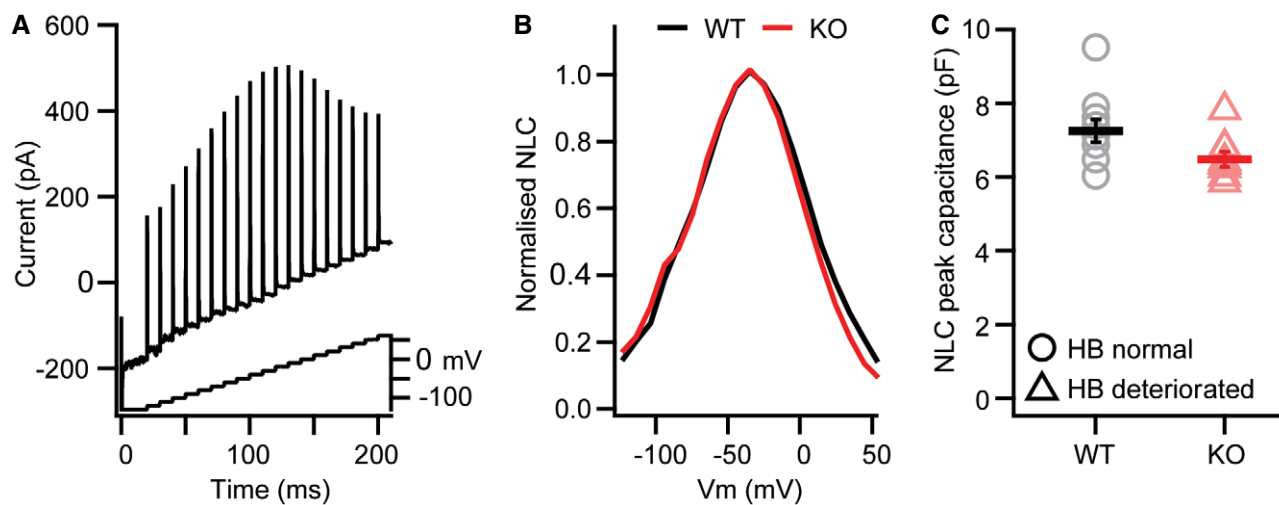


## Expanded View Figures



**Figure EV1. OHC electromotility remains unaffected in *Lrba* mutants.**

Prestin-driven electromotility remains functional in *Lrba*-KO OHCs (p15–16).

- A Motor protein levels in the OHC membrane leaflet were determined electrophysiologically by analyzing the nonlinear capacitance (NLC) of WT and *Lrba*-KO OHCs in response to a stair-step protocol.
- B, C Representative current traces to quantify; (B) NLC voltage dependence; and (C) peak capacitance. In these latter experiments, no statistically significant differences between WT and *Lrba* mutants could be detected (WT  $n = 10$ , *Lrba*-KO  $n = 9$ ;  $P = 0.063$ ; Student's  $t$ -test). Data are presented as means  $\pm$  s.e.m.

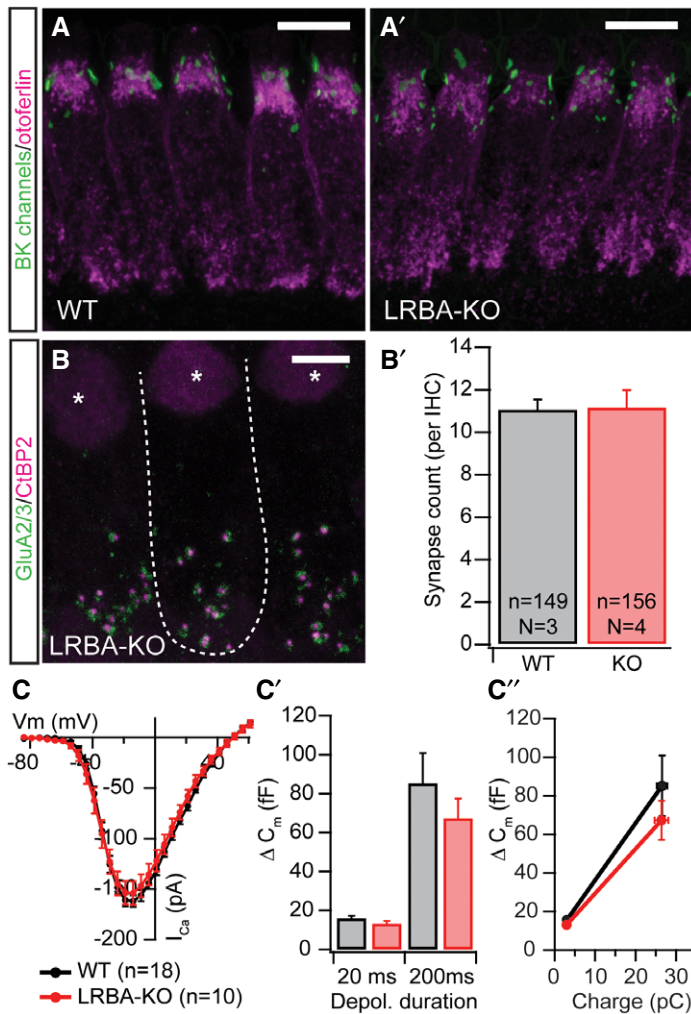
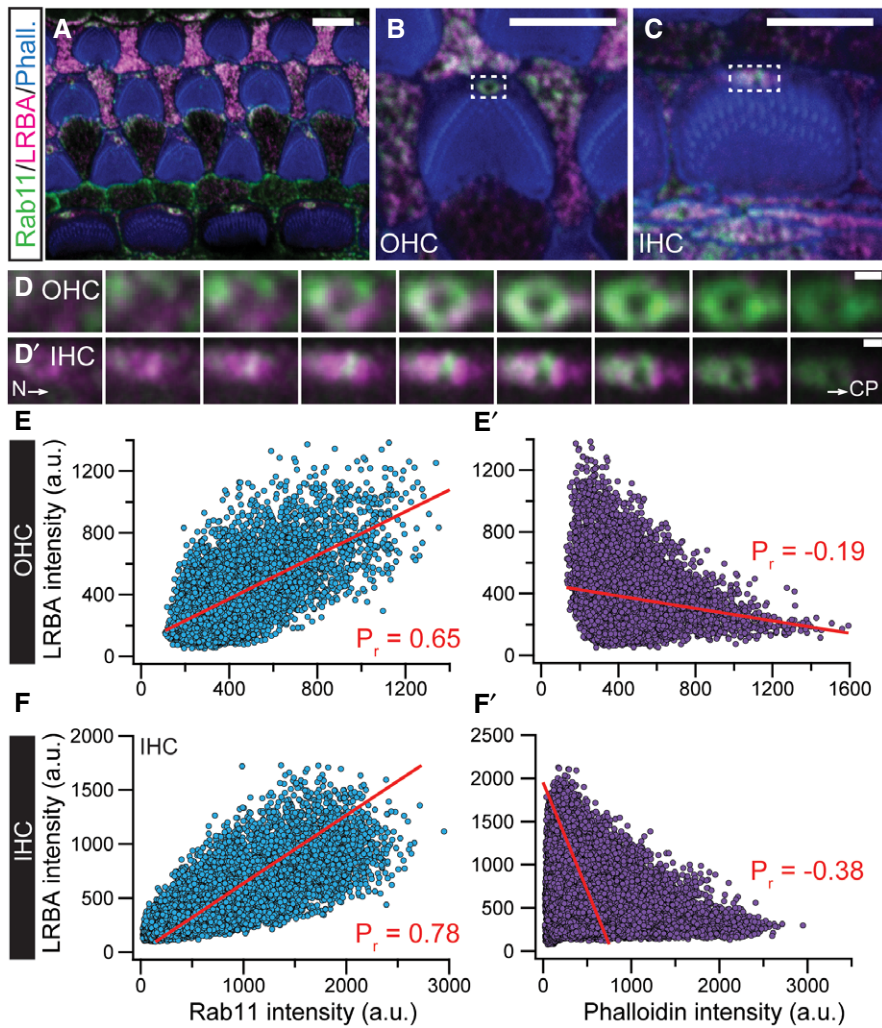


**Figure EV2. Normal maturation, synapse count, and synaptic function in *Lrba* mutant IHCs.**

**A, A'** Spotlike BK channel (green) staining at the IHC neck region indicates normal IHC maturation in *Lrba* mutant mice; IHCs have been counterstained for otoferlin (magenta). Scale bar: 5 μm.

**B, B'** Synapse count in apical turn IHCs from p14–16 WT and *Lrba*-KO mice, as assessed by presynaptic CtBP2 (magenta) and postsynaptic GluA2/3 (green) co-staining remains unaltered, as quantified in (B'). Data are presented as means ± s.e.m. The dashed line in (B) outlines a single IHC, and asterisks indicate nuclei. Scale bar: 10 μm.

**C–C''** Electrophysiologically recorded whole-cell Ca<sup>2+</sup> current–voltage relationship from p14–17 IHCs show similar voltage dependence and current amplitudes in both genotypes. (C') Exocytic ΔC<sub>m</sub> in response to step depolarizations to the respective maximum Ca<sup>2+</sup> current potential for either 20 ms (to deplete readily releasable vesicles) or 200 ms (to probe sustained exocytosis) revealed no statistically significant difference in synaptic release between WT (n = 18; N = 16) and *Lrba*-KO IHCs (n = 10; N = 7) (P = 0.24 and P = 0.51, respectively; Student's t-test). (C'') Similarly, release efficiencies for both depolarization durations (i.e., ΔC<sub>m</sub> per Q<sub>Ca2+</sub>) appear unchanged in *Lrba* mutants. Data are presented as means ± s.e.m.



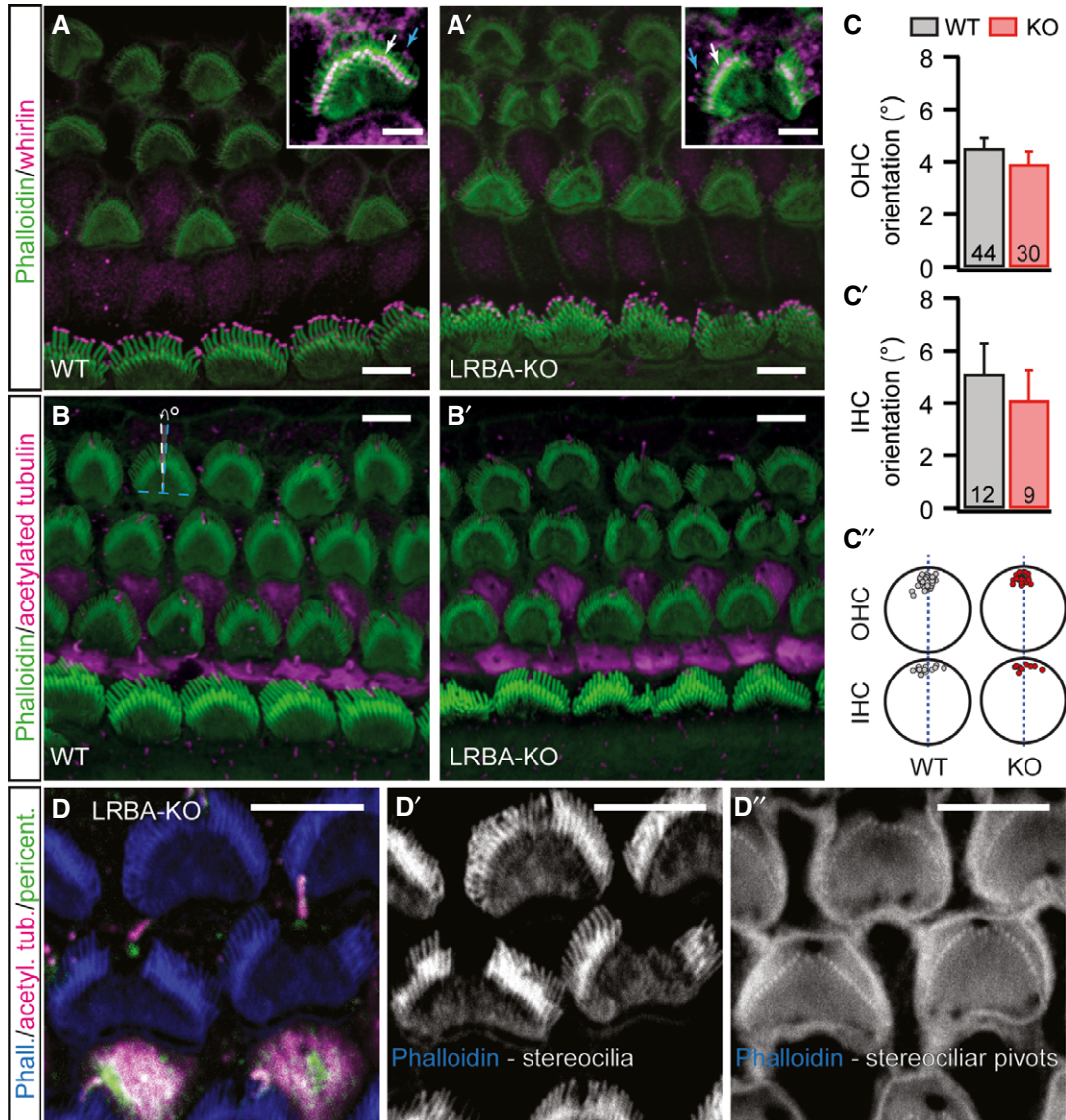


**Figure EV4. Unaltered targeting of whirlin to stereociliar tips and normal planar cell polarity in *Lrba* mutant hair cells.**

- A, A' Whirlin (magenta) is found at stereociliar tips of p8 OHCs and IHCs of both, (A) wild-type and (A') *Lrba* mutant animals (blue and white arrows in the insets indicate first- and second-row stereocilia, respectively, for representative OHCs at adjusted brightness for clarity). Stereocilia have been counterstained using fluorophore-coupled phalloidin (green). Scale bars: 5  $\mu$ m.
- B, B' *Lrba* mutant hair cells exhibit normal planar cell polarity, as assessed by calculating the degrees of deviation ( $^{\circ}$ ) from an axis perpendicular to the apico-basal axis of the organ of Corti that runs through the center of each individual hair bundle (illustrated in B for an OHC; dashed blue lines indicate the perpendicular axes, dashed white line and white arrow illustrate the degrees of deviation). Scale bars: 5  $\mu$ m.
- C–C' Quantification of the data from (B) (in C:  $P = 0.33$ , in C':  $P = 0.56$ ; Student's  $t$ -test). Numbers indicate the number of hair cells analyzed. (C'') Simplified graphical representation of the approximate kinocilia insertion points for OHCs and IHCs in wild-type and *Lrba*-KOs. Data are presented as means  $\pm$  s.e.m.
- D–D'' Basal body and kinocilium localization are unaffected by stereociliar loss in *Lrba*-KO hair cells. Regardless of the extent of stereociliar loss in *Lrba* mutants (D'), stereociliar pivot points can still be observed (D''). Samples were stained with specific antibodies against pericentrin (green; basal body) and acetylated tubulin (magenta; kinocilia) as well as fluorophore-conjugated phalloidin (blue, actin-rich stereocilia). Scale bars: 5  $\mu$ m.

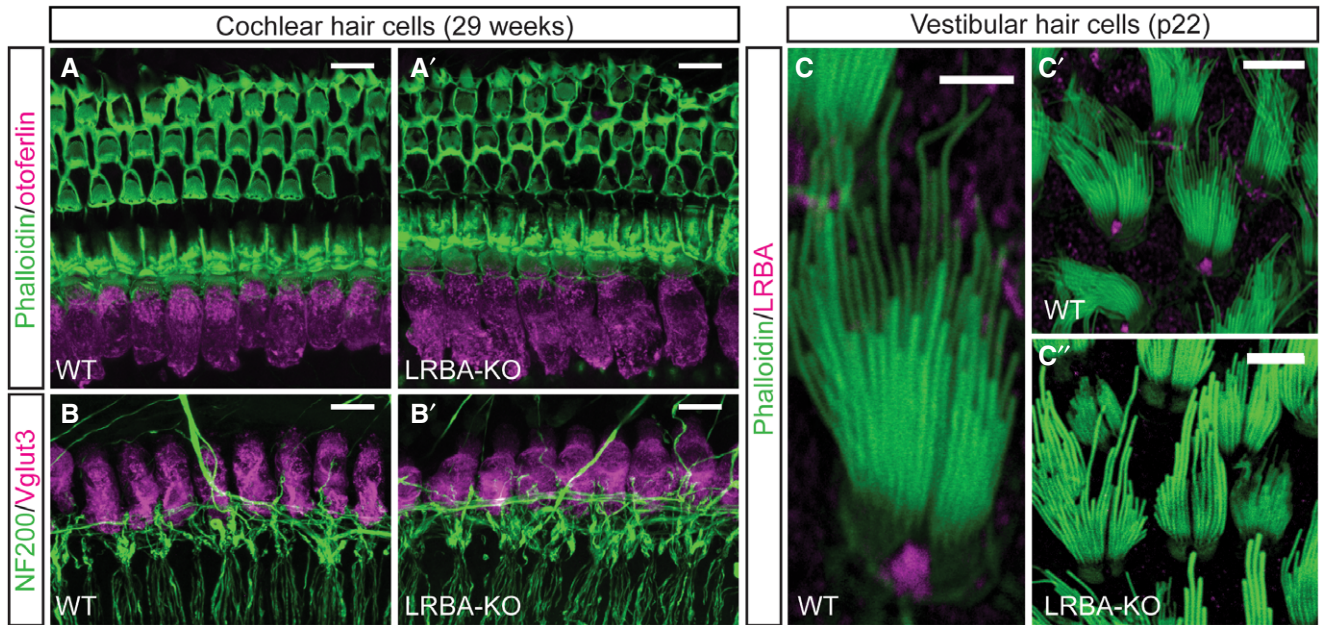


**Figure EV5. No major loss of cochlear hair cells can be observed in 29-week-old *Lrba* mutants and the afferent innervation pattern is maintained; moreover, vestibular hair cells do not show a prominent hair bundle phenotype.**

- A, A' Representative confocal maximum projections of 29-week-old (A) wild-type and (A') *Lrba*-KO organs of Corti stained with a specific antibody against the exocytic protein otoferlin (magenta). Actin-rich structures were counterstained with fluorophore-conjugated phalloidin. Scale bars: 10  $\mu$ m.
- B, B' IHC afferent innervation patterns in (B) wild-type and (B') *Lrba* mutants are maintained after 29 weeks. Specimen were stained with specific antibodies against NF200 (green; SGN afferent fibers) and the IHC-specific marker Vglut3 (magenta). Scale bars: 10  $\mu$ m.
- C–C'' Utricular hair cells also express LRBA at the foniculus, but do not show any obvious hair bundle deficits at an age where cochlear hair bundles are degenerated. (C) Detail of a single utricular hair bundle illustrating LRBA localization at the foniculus. Overviews of (C') wild-type and (C'') *Lrba*-KO hair bundles from p22 utricles. Scale bars: 5  $\mu$ m in (C); 10  $\mu$ m in (C' and C'').